JOURNAL OF GUIDANCE, CONTROL, AND DYNAMICS
Vol. 18, No. 4, July–August 1995

Estimation and Control of Tethered Satellite Systems

Ehud Netzer*
Technion City, Haifa 32000, Israel
and
Thomas R. Kane†
Stanford University, Stanford, California 94305

This paper describes the analysis of a tethered system during the station-keeping phase. The system is composed of two small satellites connected by a long tether. The satellites are modeled as particles, and the tether is represented by eight rigid, massive rods. The angles between adjacent elements can vary with time. Only measurements at the end bodies are considered, and the angles between the tether segments are estimated by using a reduced-order estimator. The compensator design is based on the linear quadratic regulator algorithm and a steady-state Kalman filter. It is shown that all motion modes are observable with the available measurements and controllable with thrusts on one of the satellites.

Nomenclature

$A, B, C, D, E, F, G, H, I$	= reference frames
$C_{i,j}$	= matrix entries
$F, \mathcal{F}, F_{aa}, F_{ab}, F_{ba}, F_{bb}$	= coefficient matrix and its partitions
$G, \mathcal{G}, G_a, G_b$	= control distribution matrix and its partitions
$H, \mathcal{H}, H_a, H_b$	= output distribution matrix and its partitions
I_T	= tether segment transverse moment of inertia
K, K_a, K_b	= full state gain matrix and its partitions
$K_{i,j}$	= matrix entries
L	= tether segment half length
L_E	= estimator gain matrix
M, M_T, M_E	= satellite, tether segment, and Earth masses
$M_{i,j}$	= matrix entries
N	= Newtonian reference frame
O	= Earth
P_1, P_2	= unmanned satellites
P_T	= tether midpoint
$Q_E^{(i)}$	= thrust spectral density
Q_x, Q_λ	= weighting matrices
q_i	= generalized coordinate
R	= nominal orbital radius
$R_E^{(i)}$	= noise spectral density
R_u	= weighting matrix
$R_1, \ldots, R_8$	= tether segments
$\mathcal{S}$	= block diagonal matrix
T_c	= transformation matrix
T_1, T_2	= thrust vector measure numbers
U	= control vector
u_i	= generalized speed
V, V_i	= noise vector and its components
v	= output error vector
w	= process noise vector
X, X_a, X_b	= state vector and its partitions
x	= distance
Y, Y_1, Y_2	= output vector and its partitions
$Z_{i,j}$	= matrix entries
α, β	= dimensionless quantities
μ	= dimensionless distance
Ξ, Ξ_c	= real and complex modal state vector
τ	= dimensionless time
Ω	= nominal orbital rate
$\bar{(\ )}$	= normalized quantity
$\hat{(\ )}$	= scaled quantity
$\check{(\ )}$	= estimated quantity

Received Jan. 28, 1992; revision received Jan. 6, 1993; accepted for publication July 28, 1993.

*Adjunct Teaching Fellow, Faculty of Mechanical Engineering.
†Professor of Applied Mechanics.

Introduction

WHENEVER one deals with a system that includes a continuous element such as a tether, the decision on how to model this element is of great importance. A simple model reduces the complexity of analysis and controller design, but important phenomena may be neglected. The tether may be modeled as (i) a rigid, massless rod; (ii) a sequence of rigid or extensible segments; and (iii) a continuous, massive, extensible or inextensible cable. As the fidelity of the model increases, so does the complexity of the analysis and the controller.

The simplest way to model the tether is as a rigid, massless rod.[1–4] By using this kind of model, one can describe the rigid-body motion of the system, but tether bending and stretching are neglected. To include the effect of the first longitudinal stretch mode, Fujii and Ishijima[5] represented the tether by an extensible, massless rod.

In the second category of models, the tether is represented by a sequence of elements, such as beads connected by rigid massless rods[6,7] or beads connected by massless springs.[8] Woodward[9] suggested a model in which the tether is modeled as a sequence of cylinders connected to one another through a special joint. All of these models allow for tether curvature and, consequently, are more realistic than those that preclude bending. To obtain high fidelity, a large number of elements must be used, which results in complex dynamics. This type of model is often used for simulation of the system behavior, but not for control design.

In the third class of models, a continuous massive tether is analyzed. The tether may be elastic[10–12] or inextensible. Usually, to deduce practical information from this kind of analysis, the equations of motion are linearized with respect to modal states, and the researcher ultimately must decide how many modes to take into account. The usual presumption is that the more modes are included, the better will the model represent the real tether. In most cases, as in the case of discrete-segment models, the controller design is based on a simple model, so that the advantage of the accurate model is largely lost, and under certain circumstances, parametric resonance of the roll motion may be induced.[10] One reason that only rigid-body motion is considered for the controller design is that measurements of states related to transverse curvature modes are not available

and need to be estimated. A paper that describes an estimation of the swing angle was presented by Swanson and Stengel[13]; however, this paper does not include a procedure to estimate curvature angles.

In the present paper, we present a model in which the tether is represented as a multisegment object, and the controller is based on the full model. Furthermore, it is assumed that only some of the states are measured while the rest are estimated. To estimate the unmeasured states, a reduced-order estimator is used with a steady-state Kalman filter.

Analytical Model and Equations of Motion

The analytical models (see Fig. 1) is based on the approach taken by Netzer and Kane,[14] in which the Shuttle, usually used as the deployer, is replaced by an unmanned satellite, and hence, the system consists of two tether-connected, unmanned satellites of approximately the same mass. The satellites are modeled as particles P_1 and P_2, each of mass M; the tether is represented by eight massive, inextensible rods $R_1, \ldots, R_8$, each of length $2L$, of transverse moment of inertia I_T, and of mass M_T, such that the total mass of the rods equals the actual mass of the tether. The angles between adjacent elements can vary with time. The system formed by P_1, P_2, and $R_1, \ldots, R_8$ is presumed to be in the gravitational field of a particle O of mass M_E (the mass of Earth) that is fixed in a Newtonian reference frame N. To avoid an overly complicated analysis, the model is planar and only in-plane motion is considered. It will be shown later that the analysis and results are also applicable to out-of-plane motion. For the same reason, the satellites are assumed to be of the same mass. Although the use of different masses for the satellites would make the problem more general, the algorithms and methods suggested in this paper would be the same.

Since the system possesses 10 degrees of freedom in N, we define generalized coordinates $q_i (i = 1, \ldots, 10)$ in conjunction with establishing a number of vector bases. The first of these is a dextral set of mutually perpendicular unit vectors $\boldsymbol{N}_i (i = 1, 2, 3)$ fixed in N (see Fig. 1), with $\boldsymbol{N}_3$ normal to the plane in which the system is intended to move. We align unit vectors $\boldsymbol{A}_i$ with $\boldsymbol{N}_i (i = 1, 2, 3)$ and subject the former triad to a dextral rigid-body rotation of amount q_1 about $\boldsymbol{N}_3$. In addition, we require that the tether center P_T lies at all times on the line that passes through O and is parallel to $\boldsymbol{A}_2$; also, we let q_2 be a dimensionless coordinate and μ a dimensionless quantity, such that $\boldsymbol{r}^{O-P_T}$, the position vector from O to P_T, is given by

$$\boldsymbol{r}^{O-P_T} = R(1 + \mu + q_2)\boldsymbol{A}_2 \tag{1}$$

Whenever q_2 vanishes and the system moves in such a way that $\dot{q}_1 = \Omega$ whereas $R_1, \ldots, R_8$ all lie on a line that is parallel to $\boldsymbol{A}_2$,

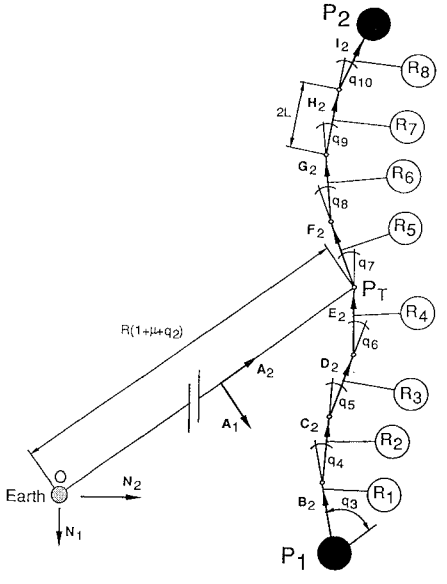

Fig. 1 Model description.

this will be called the desired motion of the system. The quantity μ is given by

$$\mu = \frac{1}{R}(x - R) \tag{2}$$

where x is governed by the equation

$$R^3\left[M_T \sum_{i=-4}^{4} \frac{1}{(x + 2iL)(x + 2iL + 2L)} + M\left(\frac{1}{(x - 8L)^2} + \frac{1}{(x + 8L)^2}\right)\right] = (8M_T + 2M)x \tag{3}$$

The quantity x is the orbital radius at which the tether midpoint would travel during the desired motion of the system. Equation (3) is obtained by calculating the centrifugal and gravitational forces acting on each element of the system. With the numerical values given later, μ is found to be 2.1×10^{-6}, so it is neglected when the linearized equations of motion are derived.

To orient the tether elements relative to $\boldsymbol{A}_i (i = 1, 2)$, we attach reference frames $B, \ldots, I$ to $R_1, \ldots, R_8$, respectively; align unit vectors $\boldsymbol{B}_i$ with $\boldsymbol{A}_i (i = 1, 2, 3)$; subject the B basis to a rotation characterized by the vector $q_3\boldsymbol{A}_3$; and repeat this procedure so that C is rotated relative to B by $q_4\boldsymbol{B}_3$, D is rotated relative to C by $q_5\boldsymbol{C}_3$, E is rotated relative to D by $q_6\boldsymbol{D}_3$, F is rotated relative to E by $q_7\boldsymbol{E}_3$, G is rotated relative to F by $q_8\boldsymbol{F}_3$, H is rotated relative to G by $q_9\boldsymbol{G}_3$, and I is rotated relative to H by $q_{10}\boldsymbol{H}_3$. Hence, the generalized coordinate q_3 is the angle between the local vertical and $\boldsymbol{B}_2$, whereas the generalized coordinates $q_i (i = 4, \ldots, 10)$ are the angles between adjacent elements.

In terms of a dimensionless time τ, defined as

$$\tau = \Omega t \tag{4}$$

the kinematic differential equations for the generalized speeds $u_1, \ldots, u_{10}$ can be written as

$$u_1 = \frac{dq_1}{d\tau} - 1, \qquad u_i = \frac{dq_i}{d\tau} \qquad (i = 2, \ldots, 10) \tag{5}$$

In addition to gravitational forces exerted by O on P_1, P_2, $R_1, \ldots, R_8$, and gravitational moments exerted by O on $R_1, \ldots, R_8$, the analytical model must accommodate control forces exerted on P_2 by means of thrusters. To this end, we introduce a thrust vector $\boldsymbol{T}$ as

$$\boldsymbol{T} = T_1\boldsymbol{I}_1 + T_2\boldsymbol{I}_2 \tag{6}$$

where $\boldsymbol{I}_1$ and $\boldsymbol{I}_2$ are unit vectors attached to R_8 (see Fig. 1) and T_1 and T_2 are functions of system states, chosen on the basis of control theory in such a way as to keep the system near the required orientation.

The exact equations of motion, generated with AUTOLEV,[15] are omitted in the interest of brevity. However, these equations may be linearized about the desired motion, in which the generalized coordinates q_i $(i = 2, \ldots, 10)$ and the generalized speeds u_i $(i = 1, \ldots, 10)$, as well as the first time derivatives of these quantities, all are equal to zero. Hence, for purposes of control system design, it suffices to work with equations of motion linearized in these variables. Before writing the linearized equations, we introduce a number of dimensionless constants and variables:

$$\alpha = L/R \tag{7}$$

$$\beta = M_T/M, \qquad \bar{I}_T = I_T/(M_T L^2) \tag{8}$$

$$\bar{T}_i = T_i/(MR\Omega^2) \qquad (i = 1, 2) \tag{9}$$

If prime denotes differentiation with respect to τ, the linearized normalized equations of motion can be written in a matrix form:

$$\left[\begin{array}{c|c|c} M_{1,1} & 0 & M_{1,j}(1\times 8) \\ 0 & M_{2,2} & 0 \\ \hline \\ M_{i,1} & 0 & M_{i,j} \\ (8\times 1) & & (8\times 8) \\ \\ \\ \\ \\ \\ \\ \end{array}\right]\left\{\begin{array}{c} u_1' \\ u_2' \\ u_3' \\ u_4' \\ u_5' \\ u_6' \\ u_7' \\ u_8' \\ u_9' \\ u_{10}' \end{array}\right\}$$

$$+\left[\begin{array}{c|c|c} 0 & C_{1,2} & 0 \\ C_{2,1} & 0 & C_{2,j}(1\times 8) \\ \hline \\ 0 & C_{i,2} & 0 \\ & (8\times 1) & \\ \\ \\ \\ \\ \\ \end{array}\right]\left\{\begin{array}{c} u_1 \\ u_2 \\ u_3 \\ u_4 \\ u_5 \\ u_6 \\ u_7 \\ u_8 \\ u_9 \\ u_{10} \end{array}\right\}$$

$$+\left[\begin{array}{c|c} 0 & K_{1,j}(1\times 8) \\ K_{2,1} & 0 \\ \hline \\ 0 & K_{i,j} \\ & (8\times 8) \\ \\ \\ \\ \\ \\ \end{array}\right]\left\{\begin{array}{c} q_2 \\ q_3 \\ q_4 \\ q_5 \\ q_6 \\ q_7 \\ q_8 \\ q_9 \\ q_{10} \end{array}\right\}=\left[\begin{array}{c|c} Z_{1,1} & 0 \\ 0 & Z_{2,2} \\ \hline \\ Z_{i,j} & 0 \\ (8\times 1) & \\ \\ \\ \\ \\ \\ \end{array}\right]\left\{\begin{array}{c} \bar{T}_1 \\ \bar{T}_2 \end{array}\right\} \tag{10}$$

Expressions for the entries of $M_{i,j}$, $C_{i,j}$, $K_{i,j}$, and $Z_{i,j}$ are given in the Appendix.

State-Space Representation

To bring the equations of motion into state variable form, we introduce a 19×1 state vector $\boldsymbol{X}$ and a 2×1 control vector $\boldsymbol{U}$, where

$$\boldsymbol{X} = [u_1, \ldots, u_{10}, \quad q_2, \ldots, q_{10}]^T \tag{11}$$

and

$$\boldsymbol{U} = [\bar{T}_1 \quad \bar{T}_2]^T \tag{12}$$

It follows that Eq. (10) can be rewritten as

$$\boldsymbol{X}' = F\boldsymbol{X} + G\boldsymbol{U} \tag{13}$$

Since the equations in (10) are complicated, the transformation to the state-space form is performed numerically with MATLAB.

For purposes of control design, it is recommended that the states and controllers be balanced, which means that the states and controllers are scaled in such a way that the significance of each one is of the same order of magnitude. With this in mind, we present the following scaled states and controllers (designated by a "hat") as

$$\hat{q}_2 = \frac{q_2}{\alpha} \tag{14}$$

$$\hat{q}_i = 100 q_i \qquad (i = 3, \ldots, 10) \tag{15}$$

$$\hat{u}_i = \frac{u_i}{\alpha} \qquad (i = 1, 2) \tag{16}$$

$$\hat{u}_i = 100 u_i \qquad (i = 3, \ldots, 10) \tag{17}$$

$$\hat{T}_i = \frac{\bar{T}_i}{\alpha} \qquad (i = 1, 2) \tag{18}$$

The scaled state vector $\hat{\boldsymbol{X}}$ and the scaled control vector $\hat{\boldsymbol{U}}$ can now be written as

$$\hat{\boldsymbol{X}} = [\hat{u}_1, \ldots, \hat{u}_{10}, \quad \hat{q}_2, \ldots, \hat{q}_{10}]^T \tag{19}$$

and

$$\hat{\boldsymbol{U}} = [\hat{T}_1 \quad \hat{T}_2]^T \tag{20}$$

and the scaled state-space representation

$$\hat{\boldsymbol{X}}' = \hat{F}\hat{\boldsymbol{X}} + \hat{G}\hat{\boldsymbol{U}} \tag{21}$$

Open-Loop Eigenvalues

To get the eigenvalues of the states matrix F, numerical values are assigned to all system parameters. Specifically, we take $M = 500$ kg, $M_T = 164/8 = 20.5$ kg, $L = 1250$ m (total tether length of 20 km), $I_T = M_T L^2/12 = 2.669 \times 10^6$ kg-m^2, $\Omega = 1.178486395 \times 10^{-3}$ rad/s, and $R = 6.598388 \times 10^6$ m. The open-loop eigenvalues are calculated to be (in multiples of Ω)

$$\begin{array}{c} 0, \quad \pm j, \quad \pm\sqrt{3}j, \quad \pm 7.32j, \quad \pm 14.35j, \quad \pm 22.04j \\ \pm 30.54j, \quad \pm 39.89j, \quad \pm 49.58j, \quad \pm 58.00j \end{array} \tag{22}$$

The first two of these eigenvalues are associated with the orbital motion, the third with rigid-body motion, and the rest with transverse curvature modes. Inspection of Eq. (22) reveals that all modes are undamped, and control action is required to produce the damping.

Available Measurements

To draw realistic conclusions from the analysis, one must use measurements that can be made in a real system. In this section, we discuss the availability and properties of measurements.

In the system under discussion (see Fig. 1), the measurements of three types of quantities are required, namely, the angular rate of the system around Earth (u_1), the satellite altitude and its first time derivative (q_2, u_2), and curvature angles of the tether elements and their time derivatives [q_i, $u_i (i = 3, \ldots, 10)$]. Usually, the orbital angular rate and the altitude can be measured very accurately and with low noise. They can be obtained by systems located on the spacecrafts (such as global positioning system [GPS] or inertial navigation system [INS]) or by external means. We assume that these measurements of the spacecraft motions determine the tether midpoint motion. Measurements of the curvature angles, on the other hand, are less readily available and are more noisy. The available measurements are of the angles between the local vertical and the direction of the tether at the attachment points to the spacecrafts (this can be done by measuring the local vertical and using an angle measurement device, such as a resolver, for the relative direction of the tether). Usually, the derivatives of these angles are also available. Hence, if $\boldsymbol{V}$ is a 4×1 noise vector, given as

$$\boldsymbol{V} = [V_1 \quad V_2 \quad V_3 \quad V_4]^T \tag{23}$$

the 7×1 output vector $\boldsymbol{Y}$ can be written

$$\boldsymbol{Y} = \begin{bmatrix} u_1 \\ u_2 \\ q_2 \\ u_3 + V_1 \\ \sum_{i=3}^{10} u_i + V_2 \\ q_3 + V_3 \\ \sum_{i=3}^{10} q_i + V_4 \end{bmatrix} \tag{24}$$

The first three components of Eq. (24) indicate perfect measurements of the orbital motion, whereas the measurements of angles and angle derivatives include the noise components $V_1, \ldots, V_4$, each with zero mean and with spectral densities $R_E^{(1)}, \ldots, R_E^{(4)}$, respectively. Knowledge of the spectral densities is required using a Kalman filter to estimate the unknown states. For an angle sensor with a root-mean-square (rms) accuracy of 0.2 crad (0.1146 deg)[16] and a noise correlation time of 3 s, the normalized spectral densities for the angle measurement noise can be approximated by[17]

$$R_E^{(3)} = R_E^{(4)} = 2(3\Omega)(0.002^2) = 2.826 \times 10^{-8} \tag{25}$$

For an angle rate sensor with an rms accuracy of 1×10^{-4} deg/s (1.745×10^{-6} rad/s)[18] and a noise correlation time of 3 s, the normalized spectral density is calculated to be

$$R_E^{(1)} = R_E^{(2)} = 2(3\Omega)(1.745 \times 10^{-6}/\Omega)^2 = 1.551 \times 10^{-8} \tag{26}$$

and the scaled spectral densities $\hat{R}_E^{(i)} (i = 1, \ldots, 4)$ are

$$\hat{R}_E^{(1)} = \hat{R}_E^{(2)} = 1.551 \times 10^{-4}, \qquad \hat{R}_E^{(3)} = \hat{R}_E^{(4)} = 2.826 \times 10^{-4} \tag{27}$$

Reduced-Order Estimator

In the previous section, it was shown that some of the states are known exactly and need not be estimated. Hence, a reduced-order estimator, for only part of the states, can be used. In Ref. 19 (pp. 352–355) a derivation of a reduced-order estimator is presented, where it is assumed that some of the states are perfectly known, whereas there is no information at all on the remaining states. As shown in Eq. (24), this is not the case for the system under discussion, since some knowledge of the other states is available. Hence, a different reduced-order estimator may be used, and its derivation is the subject of the present section.

Assume a state-space representation in the form

$$\begin{bmatrix} \dot{X}_a \\ \dot{X}_b \end{bmatrix} = \begin{bmatrix} F_{aa} & F_{ab} \\ F_{ba} & F_{bb} \end{bmatrix} \begin{bmatrix} X_a \\ X_b \end{bmatrix} + \begin{bmatrix} G_a \\ G_b \end{bmatrix} U \tag{28}$$

$$Y = \begin{bmatrix} Y_1 \\ Y_2 \end{bmatrix} = \begin{bmatrix} I & 0 \\ H_a & H_b \end{bmatrix} \begin{bmatrix} X_a \\ X_b \end{bmatrix} \tag{29}$$

where X_a is an $n_1 \times 1$ accurately measured state vector; X_b is an $n_2 \times 1$ partially measured state vector; U is an $s \times 1$ control vector; and Y_1, Y_2 are $n_1 \times 1$ and $p \times 1$ vectors, respectively.

Solving for $\dot{X}_b$ from Eq. (28) and for $H_b X_b$ from Eq. (29), we get

$$\dot{X}_b = F_{bb} X_b + \underbrace{F_{ba} X_a + G_b U}_{\text{known input}} \tag{30}$$

and

$$H_b X_b = Y_2 - H_a Y_1 \tag{31}$$

Now, the following substitutions can be used in the full estimator equations (Ref. 19, pp. 344–346) to get the estimation of X_b:

$$X_b \rightarrow X \tag{32}$$

$$F_{bb} \rightarrow F \tag{33}$$

$$F_{ba} X_a + G_b U \rightarrow GU \tag{34}$$

$$Y_2 - H_a Y_1 \rightarrow Y \tag{35}$$

$$H_b \rightarrow H \tag{36}$$

With these substitutions, the differential equation for the estimated vector $\check{X}_b$ is given as

$$\dot{\check{X}}_b = F_{bb} \check{X}_b + \underbrace{F_{ba} Y_1 + G_b U}_{\text{input}} + L_E \underbrace{(Y_2 - H_a Y_1}_{\text{measurement}} - H_b \check{X}_b) \tag{37}$$

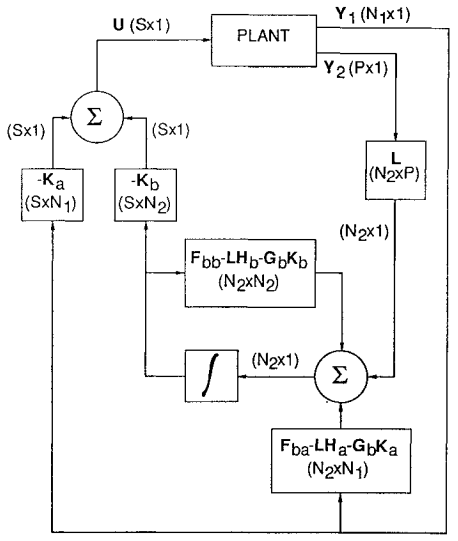

Fig. 2 Reduced-order estimator, block diagram.

where L_E is the $n_2 \times p$ estimator gain matrix. The estimator equation can also be expressed in terms of the states as

$$\dot{\check{X}}_b = (F_{bb} - L_E H_b)\check{X}_b + F_{ba} X_a + L_E H_b X_b + G_b U \tag{38}$$

The control law is based on the known states X_a and the estimated states $\check{X}_b$ in the form

$$U = -[K_a \quad K_b] \begin{bmatrix} X_a \\ \check{X}_b \end{bmatrix} \tag{39}$$

where K_a and K_b are the partitions of the full state gain matrix K. Combining Eqs. (28), (29), (38), and (39), one arrives at the equations for the closed-loop system that include an estimator and a controller,

$$\begin{bmatrix} \dot{X}_a \\ \dot{X}_b \\ \dot{\check{X}}_b \end{bmatrix} = \begin{bmatrix} F_{aa} - G_a K_a & F_{ab} & -G_a K_b \\ F_{ba} - G_b K_a & F_{bb} & -G_b K_b \\ F_{ba} - G_b K_a & L_E H_b & F_{bb} - L_E H_b - G_b K_b \end{bmatrix} \begin{bmatrix} X_a \\ X_b \\ \check{X}_b \end{bmatrix} \tag{40}$$

whereas the output vector is the same as in Eq. (29). The characteristic equation of the reduced-order estimator is

$$\det[sI - F_{bb} + L_E H_b] = 0 \tag{41}$$

The implementation of the closed-loop system is shown in the block diagram in Fig. 2. It should be noted that although H_a does not show up in Eq. (40), it shows up in the implementation since there is no information about $H_b X_b$ by itself but only as a part of Y_2.

In the system being considered here, the above reduced-order estimator is used to estimate q_i and $u_i (i = 3, \ldots, 10)$, whereas u_1, u_2, q_2 are assumed to be measured perfectly.

Real Modal State Representation, Controllability, and Observability

The linear quadratic regulator (LQR) technique to design a controller can be used only if the system is controllable with available actuators. Similarly, the linear quadratic Gaussian (LQG) technique to design the estimator applies only if the states are observable with available outputs. In this section, the equations of motion are rewritten in terms of modal coordinates, and the system controllability and observability are checked.

The transformation from the scaled state-space vector $\hat{X}$ to the complex modal state vector Ξ_c is given by[17]

$$\Xi_c = T_c^{-1} \hat{X} \tag{42}$$

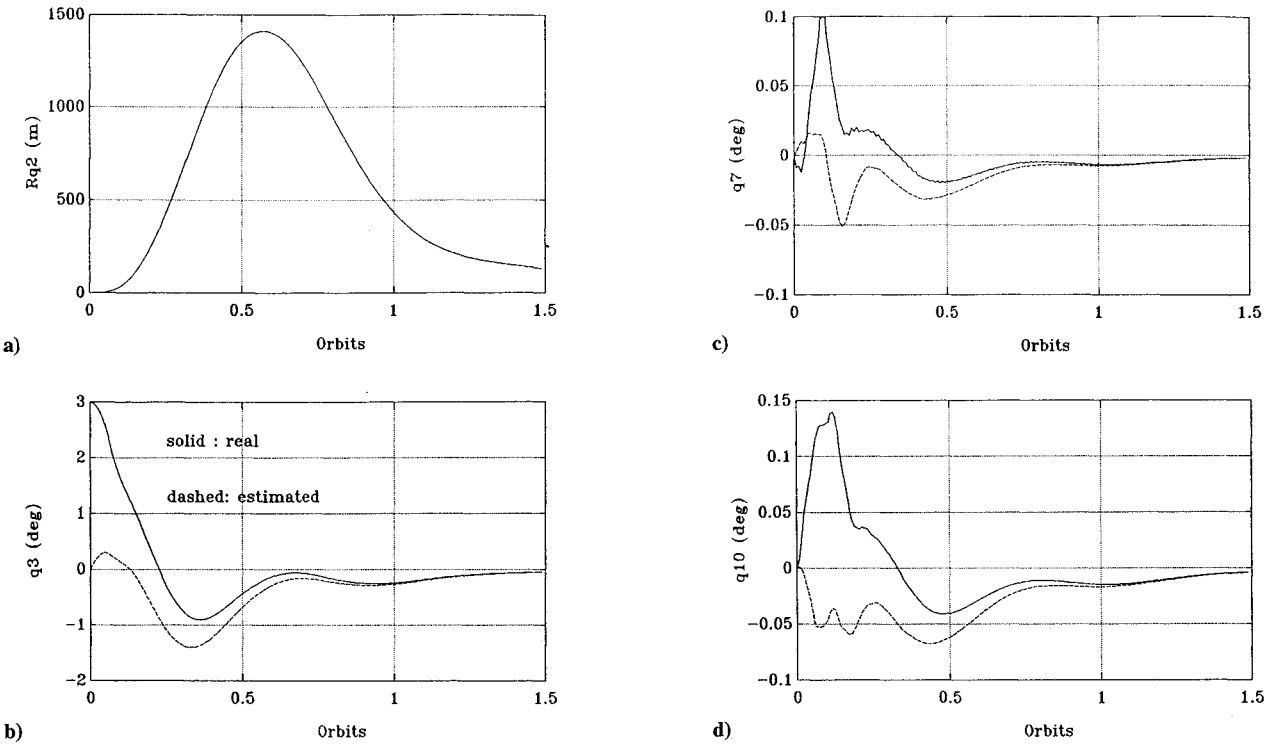

Fig. 3 Simulation results, $q_3(0) = 3$ deg, state histories: a) range deviation Rq_2, b) q_3, c) q_7, and d) q_{10}, roll deviation angles q_6 and q_7.

where T_c is a matrix whose columns are the eigenvectors of $\hat{F}$. The transformation from the complex modal state vector Ξ_c to the real modal state vector Ξ is given by

$$\Xi = \mathcal{S}^{-1}\Xi_c \tag{43}$$

where $\mathcal{S}$ is a block-diagonal matrix with unity blocks for real eigenvalues and

$$\frac{1}{2}\begin{bmatrix} 1 & -j \\ 1 & j \end{bmatrix} \tag{44}$$

blocks for complex eigenvalues. Hence, Eq. (21) can be written in terms of real modal coordinates as

$$\Xi' = \mathcal{F}\Xi + \mathcal{G}\hat{U} \tag{45}$$

where

$$\mathcal{F} = \mathcal{S}^{-1}T_c^{-1}\hat{F}T_c\mathcal{S} \tag{46}$$

$$\mathcal{G} = \mathcal{S}^{-1}T_c^{-1}\hat{G} \tag{47}$$

and $\mathcal{G}$ is the control distribution matrix. Similarly, Eq. (29) can be written as

$$\boldsymbol{Y} = \mathcal{H}\Xi + \boldsymbol{V} \tag{48}$$

where $\mathcal{H}$ is the observation distribution matrix, given by

$$\mathcal{H} = HST_c \tag{49}$$

Since the eigenvalues in Eq. (22) are distinct, the controllability can be checked by inspecting $\mathcal{G}$ and the observability by inspecting $\mathcal{H}$. It was found that, indeed, all transverse curvature modes are controllable by T_1 and observable by the available measurements.

Compensator Design

The combination of the controller with the reduced-order estimator produces the compensator. In this section, the compensator parameters are presented. The design of the compensator can be carried out when the equations of motion are written in terms of generalized coordinates, as in Eq. (21), as well as when they are written in terms of modal coordinates, as in Eq. (45). The former form is chosen, but the weights are given in terms of the eigenvalues.

The LQR procedure is used to calculate the 2×19 optimal gain matrix K such that the control law

$$\boldsymbol{U} = -K\boldsymbol{X} \tag{50}$$

minimizes the cost function

$$J = \int_{t_0}^{t_f} \left(\boldsymbol{X}^T Q_x \boldsymbol{X} + \boldsymbol{U}^T R_u \boldsymbol{U}\right) \mathrm{d}t \tag{51}$$

where Q_x and R_u are 19×19 and 2×2 weighting matrices, respectively. To gain better control on the mode dampings, the states are weighted in terms of modal coordinates by the matrix Q_λ and later are transferred to generalized coordinate representation through the transformation

$$Q_x = \left(\mathcal{S}^{-1}T_c^{-1}\right)^T Q_\lambda \left(\mathcal{S}^{-1}T_c^{-1}\right) \tag{52}$$

To obtain sufficient damping in the higher modes, we chose higher weights for these modes, so that the weighting matrices Q_λ and R_u are

$$\begin{aligned} Q_\lambda = \text{ diag}[&0.5, \quad 0.2(\times 2), \quad 0.1(\times 2), \quad 0.2(\times 2) \\ &0.2(\times 2), \ldots, 0.2(\times 2), \quad 0.2(\times 2) \\ &0.2(\times 2), \quad 0.3(\times 2), \quad 0.6(\times 2)] \end{aligned} \tag{53}$$

$$R_u = \text{diag}[1.5, \quad 0.5] \tag{54}$$

The multiplications by 2 in Eq. (53) indicate a weight for a pair of conjugate complex eigenvalues; these weights are ordered in correspondence with the order of the eigenvalues in Eq. (22).

The system closed-loop eigenvalues are found to be (in multiples of Ω)

$$\begin{aligned} &-0.49, \quad -0.47 \pm 1.02j, \quad -0.69 \pm 1.67j, \quad -2.62 \pm 7.37j \\ &-2.12 \pm 14.37j, \quad -2.86 \pm 22.16j, \quad -3.95 \pm 30.69j \\ &-4.22 \pm 40.05j, \quad -5.38 \pm 49.73j, \quad -4.68 \pm 57.14j \end{aligned} \tag{55}$$

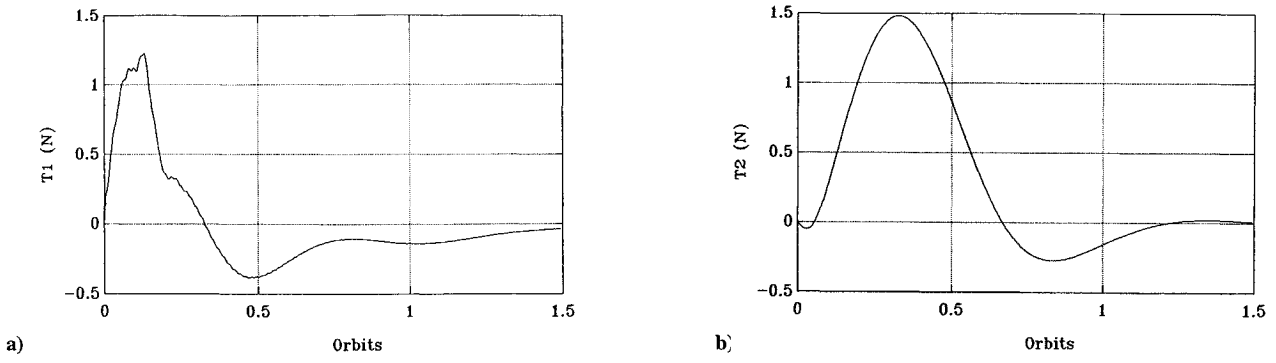

Fig. 4 Simulation results, $q_3(0) = 3$ deg, thrust histories: a) T_1 and b) T_2.

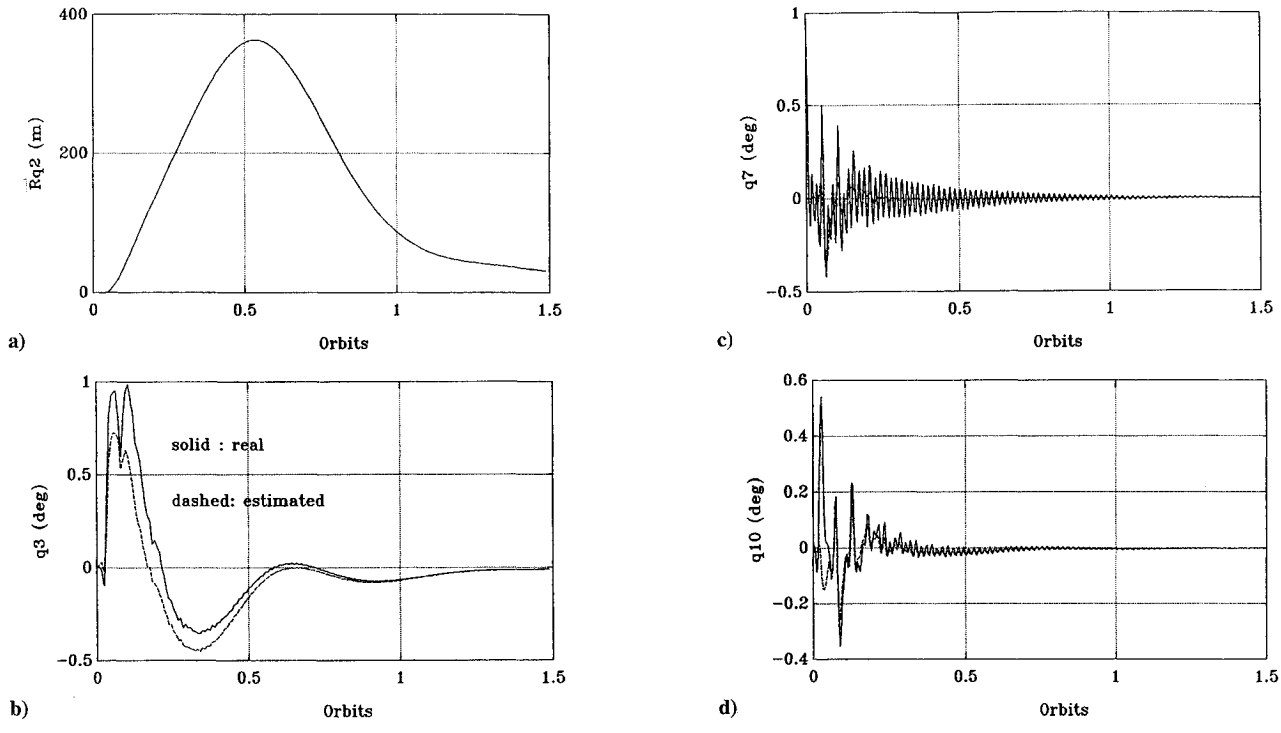

Fig. 5 Simulation results, $q_7(0) = 1$ deg, state histories: a) range deviation Rq_2, b) q_3, c) q_7, and d) q_{10}, roll deviation angles q_6 and q_7.

Since the ratio of the real part to the imaginary part indicates the damping of the specific mode, it is clear from Eq. (55) that reasonable damping has been achieved for all eigenvalues. The damping can be improved if lower weights are specified for the thrusts.

The LQG technique is used to calculate the 16×4 optimal estimator gain matrix L such that the estimator equation [see Eq. (38)] minimizes the cost function

$$J_E = \int_{t_0}^{t_f} \left(v^T R_E v + w^T Q_E w\right) \mathrm{d}t \tag{56}$$

where v is the output error vector given by

$$v = Y_2 - H_b X_b \tag{57}$$

and w is the process noise vector. To execute this procedure, the spectral density of the process noise, in addition to the noise spectral densities given in Eq. (27), is required. It is assumed that the process noise is due to thrust inaccuracies. If the thrust accuracy is 0.1 N rms with a correlation time of 100 s, then $Q_E^{(1)}$ and $Q_E^{(2)}$, the normalized spectral densities of the thrust components noise, are given by

$$Q_E^{(1)} = Q_E^{(2)} = 2(100\Omega)(0.1/MR\Omega^2)^2 = 1.125 \times 10^{-10} \tag{58}$$

and the scaled spectral densities are

$$\hat{Q}_E^{(1)} = \hat{Q}_E^{(2)} = Q_E^{(1)}/\alpha^2 = 3.135 \times 10^{-3} \tag{59}$$

With these values, the estimator closed-loop eigenvalues are found to be (in multiples of Ω)

$$\begin{gathered} -0.74, \quad -1.93 \pm 4.01j, \quad -2.08 \pm 11.39j, \quad -2.10 \pm 19.38j \\ -2.04 \pm 28.22j, \quad -1.81 \pm 38.04j, \quad -1.25 \pm 48.43j \\ -0.45 \pm 57.60j, \quad -2250 \end{gathered} \tag{60}$$

From Eq. (60) one can see that the estimation errors for the lower eigenvalues are damped better than the higher eigenvalues.

Clearly, the eight-segment model under consideration provides only an approximation to the real tether. Hence, the robustness of the compensator to uncertainties in the model, especially for the high-frequency region, should be checked. This is left for future analysis.

Simulation Results

To test the compensator, the response of the system to nonzero initial values is simulated. The simulation is performed using the full

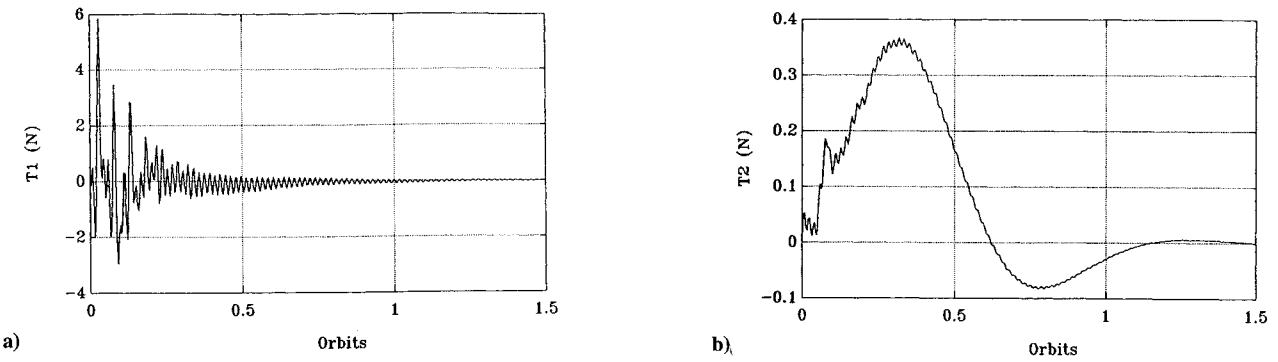

Fig. 6 Simulation results, $q_7(0) = 1$ deg, thrust histories: a) T_1 and b) T_2.

nonlinear equations that have been generated with AUTOLEV. The system response to two initial condition vectors has been simulated; in the first case, $q_3(0) = 3$ deg, and in the second case, $q_7(0) = 1$ deg. The first case corresponds to a perturbation of the rigid-body mode, whereas in the second case all the transverse curvature modes are excited. In both cases, all the initial estimated states are set to zero. The simulation results for the first case are presented in Figs. 3 and 4, and the results for the second case in Figs. 5 and 6.

Case 1: $q_3(0) = 3$ deg. The maximum range deviation Rq_2 is 1400 m (Fig. 3a); q_3 is damped with an overshoot of 30% (Fig. 3b); the maximum values of q_7 and q_{10} are 0.09 deg and 0.13 deg, respectively (Figs. 3c and 3d), which indicate that the tether remains nearly straight throughout the maneuver. The states are damped within 1.5 orbits, while the estimator errors are damped faster, i.e., within 0.95 orbit. The thrust histories, shown in Fig. 4, reveal a maximum of 1.3 N for T_1 and 1.5 N for T_2.

Case 2: $q_7(0) = 1$ deg. The maximum range deviation Rq_2 is 400 m (Fig. 5a); q_3 attains a maximum value of 1 deg (Fig. 5b); q_7 is damped within 1 orbit (Fig. 5c); and the maximum value of q_{10} is 0.5 deg (Fig. 5d). The states are damped within 1.5 orbits, whereas the estimator errors are damped faster, i.e., within 0.9 orbit. The thrust histories, displayed in Fig. 6, show a maximum of 6 N for T_1 and 0.4 N for T_2.

In both cases, the orbital motion of the system, represented by the histories of Rq_2 in Figs. 3a and 5a, is perturbed in the process of damping the initial values of q_3 and q_7. These results show that the orbital motion, the rigid-body mode, and the transverse curvature modes are coupled and must be treated simultaneously. Comparison of the two cases shows that although a perturbation of the curvature modes, as in Case 2, excites the rigid-body mode (Figs. 5b–5d), a perturbation of the rigid-body mode, as in Case 1, does not excite the curvature modes.

It is obvious that the compensator handles the rigid-body mode better than the higher curvature modes, as was to be expected from Eq. (55). In addition, the damping of the highest estimator mode is low [see Eq. (60)], and this is the main reason for the oscillations shown in Fig. 5c. Once the estimator errors are damped, the dominating poles are those in Eq. (55) rather than those in Eq. (60), which are less damped.

The thrust histories (Figs. 4 and 6) show that the use of T_1 is similar to that of T_2 for the rigid-body mode perturbation, as in Case 1, but it is much greater than that of T_2 for Case 2. In general, some aspects of the system response can be improved by expending more fuel.

Together, Figs. 3–6 show that the unknown states can be successfully estimated, and the system can be controlled so that the desired motion is obtained. The analysis for out-of-plane motion is very similar to that presented in this paper, because the available measurements are the same as those presented earlier for in-plane motion, and the appropriate thrust component can control all out-of-plane curvature modes as T_1 can control all in-plane curvature modes.

Conclusion

The paper describes a method to control the motion of two bodies connected by a long tether. The model takes into account the orbital motion of the system, the pendulum-like motion, and the deviation of the tether from a straight line.

An algorithm to estimate the curvature angles of the tether has been presented. The algorithm makes use of a modified reduced-order estimator in which some of the states are perfectly known and some information of the other states is available. It is shown that the system is observable with measurements only at the end bodies and is controllable with thrusts on only one end body. The results obtained in the paper are applicable to out-of-plane motion as for in-plane motion.

Appendix: Equations of Motion, Entries

$$
\begin{aligned}
M_{i,j} &= M_{j,i} \qquad (i, j \neq 1, 3)\\
M_{1,1} &= 2(1 + 64\alpha^2) + 8\bar{I}_T\alpha^2 + 2\beta(84\alpha^2 + 4)\\
M_{1,2} &= 0\\
M_{1,3} &= M_{3,1}\alpha^2 = M_{3,3}\alpha^2 = \alpha^2(128 + 168\beta + 8\bar{I}_T)\\
M_{1,4} &= M_{4,1}\alpha = \alpha[2 + 112\alpha + \beta(1 + 161\alpha) + 7\alpha\bar{I}_T]\\
M_{1,5} &= M_{5,1}\alpha = \alpha[4 + 96\alpha + \beta(4 + 142\alpha) + 6\alpha\bar{I}_T]\\
M_{1,6} &= M_{6,1}\alpha = \alpha[6 + 80\alpha + \beta(9 + 115\alpha) + 5\alpha\bar{I}_T]\\
M_{1,7} &= M_{7,1}\alpha = \alpha[8 + 64\alpha + \beta(16 + 84\alpha) + 4\alpha\bar{I}_T]\\
M_{1,8} &= M_{8,1}\alpha = \alpha[6 + 48\alpha + \beta(9 + 53\alpha) + 3\alpha\bar{I}_T]\\
M_{1,9} &= M_{9,1}\alpha = \alpha[4 + 32\alpha + \beta(4 + 26\alpha) + 2\alpha\bar{I}_T]\\
M_{1,10} &= M_{10,1}\alpha = \alpha[2 + 16\alpha + \beta(1 + 7\alpha) + \alpha\bar{I}_T]\\
M_{2,2} &= 2 + 8\beta\\
M_{3,4} &= M_{4,3}/\alpha = 112 + 161\beta + 7\bar{I}_T\\
M_{3,5} &= M_{5,3}/\alpha = 96 + 142\beta + 6\bar{I}_T\\
M_{3,6} &= M_{6,3}/\alpha = 80 + 115\beta + 5\bar{I}_T\\
M_{3,7} &= M_{7,3}/\alpha = 64 + 84\beta + 4\bar{I}_T\\
M_{3,8} &= M_{8,3}/\alpha = 48 + 53\beta + 3\bar{I}_T\\
M_{3,9} &= M_{9,3}/\alpha = 32 + 26\beta + 2\bar{I}_T\\
M_{3,10} &= M_{10,3}/\alpha = 16 + 7\beta + \bar{I}_T\\
M_{4,4} &= \alpha(100 + 155\beta + 7\bar{I}_T)\\
M_{4,5} &= \alpha(88 + 138\beta + 6\bar{I}_T)\\
M_{4,6} &= \alpha(76 + 113\beta + 5\bar{I}_T)\\
M_{4,7} &= M_{5,7} = M_{6,7} = M_{7,7} = \alpha(64 + 84\beta + 4\bar{I}_T)\\
M_{4,8} &= M_{5,8} = M_{6,8} = M_{7,8} = \alpha(48 + 53\beta + 3\bar{I}_T)\\
M_{4,9} &= M_{5,9} = M_{6,9} = M_{7,9} = \alpha(32 + 26\beta + 2\bar{I}_T)\\
M_{4,10} &= M_{5,10} = M_{6,10} = M_{7,10} = \alpha(16 + 7\beta + \bar{I}_T)\\
M_{5,5} &= \alpha(80 + 126\beta + 6\bar{I}_T)\\
M_{5,6} &= \alpha(72 + 107\beta + 5\bar{I}_T)\\
M_{6,6} &= \alpha(68 + 97\beta + 5\bar{I}_T)\\
M_{8,8} &= \alpha(36 + 35\beta + 3\bar{I}_T)\\
M_{8,9} &= \alpha(24 + 18\beta + 2\bar{I}_T)
\end{aligned}
$$

$$M_{8,10} = \alpha(12 + 5\beta + \bar{I}_T)$$
$$M_{9,9} = \alpha(16 + 10\beta + 2\bar{I}_T)$$
$$M_{9,10} = \alpha(8 + 3\beta + \bar{I}_T)$$
$$M_{10,10} = \alpha(4 + \beta + \bar{I})$$
$$C_{1,2} = -C_{2,1} = 4 + 16\beta$$
$$C_{2,4} = C_{2,10} = -C_{4,2}\alpha = -C_{10,2}\alpha = -\alpha(4 + 2\beta)$$
$$C_{2,5} = C_{2,9} = -C_{5,2}\alpha = -C_{9,2}\alpha = -\alpha(8 + 8\beta)$$
$$C_{2,6} = C_{2,8} = -C_{6,2}\alpha = -C_{8,2}\alpha = -\alpha(12 + 18\beta)$$
$$C_{2,7} = -C_{7,2}\alpha = -\alpha(16 + 32\beta)$$
$$K_{1,3} = 24\alpha^2\bar{I}_T$$
$$K_{1,4} = 3\alpha^2\bar{I}_T(7 - 22\alpha)$$
$$K_{1,5} = 3\alpha^2\bar{I}_T(6 - 40\alpha)$$
$$K_{1,6} = 3\alpha^2\bar{I}_T(5 - 54\alpha)$$
$$K_{1,7} = 3\alpha^2\bar{I}_T(4 - 64\alpha)$$
$$K_{1,8} = 3\alpha^2\bar{I}_T(3 - 54\alpha)$$
$$K_{1,9} = 3\alpha^2\bar{I}_T(2 - 40\alpha)$$
$$K_{1,10} = 3\alpha^2\bar{I}_T(1 - 22\alpha)$$
$$K_{2,2} = -6(1 + 4\beta)$$
$$K_{3,3} = 384 + 504\beta + 24\bar{I}_T$$
$$K_{3,4} = 336 + 483\beta + 3(7 - 22\alpha)\bar{I}_T$$
$$K_{3,5} = 288 + 426\beta + 3(6 - 40\alpha)\bar{I}_T$$
$$K_{3,6} = 240 + 345\beta + 3(5 - 54\alpha)\bar{I}_T$$
$$K_{3,7} = K_{4,7} = K_{5,7} = K_{6,7} = K_{7,3} = K_{7,4} = K_{7,5} = K_{7,6} = K_{7,7} = 192 + 252\beta + 3(4 - 64\alpha)\bar{I}_T$$
$$K_{3,8} = K_{4,8} = K_{5,8} = K_{6,8} = K_{7,8} = 144 + 159\beta + 3(3 - 54\alpha)\bar{I}_T$$
$$K_{3,9} = K_{4,9} = K_{5,9} = K_{6,9} = K_{7,9} = 96 + 78\beta + 3(2 - 40\alpha)\bar{I}_T$$
$$K_{3,10} = K_{4,10} = K_{5,10} = K_{6,10} = K_{7,10} = 48 + 21\beta + 3(1 - 22\alpha)\bar{I}_T$$
$$K_{4,3} = \alpha[336 + 483\beta + 3(7 - 28\alpha)\bar{I}_T]$$
$$K_{4,4} = \alpha[336 - 228\alpha + 483\beta - 126\alpha\beta + 3(7 - 28\alpha)\bar{I}_T]$$
$$K_{4,5} = \alpha[288 - 192\alpha + 426\beta - 84\alpha\beta + 3(6 - 44\alpha)\bar{I}_T]$$
$$K_{4,6} = \alpha[240 - 96\alpha + 345\beta - 42\alpha\beta + 3(5 - 56\alpha)\bar{I}_T]$$
$$K_{5,3} = \alpha[288 + 426\beta + 3(6 - 48\alpha)\bar{I}_T]$$
$$K_{5,4} = \alpha[288 - 192\alpha + 426\beta - 86\alpha\beta + 3(6 - 48\alpha)\bar{I}_T]$$
$$K_{5,5} = \alpha[288 - 384\alpha + 426\beta - 321\alpha\beta + 3(6 - 48\alpha)\bar{I}_T]$$
$$K_{5,6} = \alpha[240 - 192\alpha + 345\beta - 156\alpha\beta + 3(5 - 58\alpha)\bar{I}_T]$$
$$K_{6,3} = \alpha[240 + 345\beta + 3(5 - 60\alpha)\bar{I}_T]$$
$$K_{6,4} = \alpha[240 - 96\alpha + 345\beta - 42\alpha\beta + 3(5 - 60\alpha)\bar{I}_T]$$
$$K_{6,5} = \alpha[240 - 192\alpha + 345\beta - 156\alpha\beta + 3(5 - 60\alpha)\bar{I}_T]$$
$$K_{6,6} = \alpha[240 - 288\alpha + 345\beta - 318\alpha\beta + 3(5 - 60\alpha)\bar{I}_T]$$
$$K_{8,3} = K_{8,4} = K_{8,5} = K_{8,6} = K_{8,7} = \alpha[144 + 159\beta + 3(3 - 60\alpha)\bar{I}_T]$$
$$K_{8,8} = \alpha[144 + 288\alpha + 159\beta + 318\alpha\beta + 3(3 - 54\alpha)\bar{I}_T]$$
$$K_{8,9} = \alpha[96 + 192\alpha + 78\beta + 156\alpha\beta + 3(2 - 40\alpha)\bar{I}_T]$$
$$K_{8,10} = \alpha[48 + 96\alpha + 21\beta + 42\alpha\beta + 3(1 - 22\alpha)\bar{I}_T]$$
$$K_{9,3} = K_{9,4} = K_{9,5} = K_{9,6} = K_{9,7} = \alpha[96 + 78\beta + 3(2 - 48\alpha)\bar{I}_T]$$
$$K_{9,8} = \alpha[96 + 192\alpha + 78\beta + 156\alpha\beta + 3(2 - 44\alpha)\bar{I}_T]$$
$$K_{9,9} = \alpha[96 + 384\alpha + 78\beta + 312\alpha\beta + 3(2 - 40\alpha)\bar{I}_T]$$
$$K_{9,10} = \alpha[48 + 192\alpha + 21\beta + 84\alpha\beta + 3(1 - 22\alpha)\bar{I}_T]$$
$$K_{10,3} = K_{10,4} = K_{10,5} = K_{10,6} = K_{10,7} = \alpha[48 + 21\beta + 3(1 - 28\alpha)\bar{I}_T]$$
$$K_{10,8} = \alpha[48 + 96\alpha + 21\beta + 42\alpha\beta + 3(1 - 26\alpha)\bar{I}_T]$$
$$K_{10,9} = \alpha[48 + 192\alpha + 21\beta + 84\alpha\beta + 3(1 - 24\alpha)\bar{I}_T]$$
$$K_{10,10} = \alpha[48 + 288\alpha + 21\beta + 126\alpha\beta + 3(1 - 22\alpha)\bar{I}_T]$$
$$Z_{1,1} = -(1 + 8\alpha)$$
$$Z_{2,2} = 1$$
$$Z_{3,1} = Z_{4,1} = Z_{5,1} = Z_{6,1} = Z_{7,1} = -8$$
$$Z_{8,1} = -6$$
$$Z_{9,1} = -4$$
$$Z_{10,1} = -2$$

References

[1]Rupp, C. C., "A Tether Tension Control Law for Tethered Subsatellites Deployed Along Local Vertical," NASA TMX-73314, 1976.

[2]Bainum, P. M., and Kumar, V. K., "Optimal Control of the Shuttle-Tethered-Subsatellite System," *Acta Astonautica*, Vol. 7, May 1980, pp. 1333–1348.

[3]Modi, V. J., Chang-Fu, G., Misra, A. K., and Xu, D. M., "On the Control of the Space Shuttle Based Tethered Systems," *ACTA Astronautica*, Vol. 9, No. 6–7, 1982, pp. 437–443.

[4]Davis, W. R., and Banerjee, A. K., "Libration Damping of a Tethered Satellite by Yo-Yo Control with Angle Measurement," *Journal of Guidance, Control, and Dynamics*, Vol. 13, No. 2, 1990, pp. 370–374.

[5]Fujii, H. and Ishijima, S., "Mission Function Control for Deployment and Retrieval of a Subsatellite," *Journal of Guidance, Control, and Dynamics*, Vol. 12, No. 2, 1989, pp. 243–247.

[6]Fujii, H., Kokubun, K., and Uchiyama, K., "Control of Deployment/Retrieval of Subsatellite Connected by Flexible Tether," *AIAA Journal*, 1989.

[7]No, T. S., and Cochran, J. E., "Dynamics and Control of a Tethered Flight Vehicle," AAS/AIAA Astrodynamics Specialist Conference (Durango, CO), Aug. 1991, AAS Paper 91-544.

[8]Banerjee, A. K., "Dynamics of Tethered Payloads with Deployment Rate Control," *Journal of Guidance, Control, and Dynamics*, Vol. 13, No. 4, 1990, pp. 759–762.

[9]Woodward, G., *A Simulation Program For Tethered Systems*, Ph.D. Dissertation, Stanford Univ., Stanford, CA, 1991.

[10]Bainum, P. M., Diarra, C. M., and Kumar, V. K., "Shuttle-Tethered Subsatellite System Stability with a Flexible Massive Tether," *Journal of Guidance, Control, and Dynamics*, Vol. 8, No. 2, 1985, pp. 230–234.

[11]Engelstad, R. L., and Lovell, E. G., "Tether Dynamics and Vibrations Analysis," *Second International Conference on Tethers in Space, Conference Proceedings*, Vol. 14, Società Italiana di Fisica, Venice, Italy, 1986, pp. 169–173.

[12]Xu, D. M., Misra, A. K., and Modi, V. J., "Thruster-Augmented Active Control of a Tethered Subsatellite System During Its Retrieval," *Journal of Guidance, Control, and Dynamics*, Vol. 9, No. 6, 1986, pp. 663–672.

[13]Swanson, D. S., and Stengel, R. F., "Optimal State Estimation of a Tethered Satellite System," *Second International Conference on Tethers in Space, Conference Proceedings*, Vol. 14, Società Italiana di Fisica, Venice, Italy, 1986, pp. 85–92.

[14]Netzer, E., and Kane, T. R., "An Alternate Approach to Space Missions Involving a Long Tether," *Journal of the Astronautical Sciences*, Vol. 40, No. 3, 1992, pp. 313–327.

[15]Schaechter, D. B., Levinson, D. A., and Kane., T. R., *AUTOLEV User's Manual*, OnLine Dynamics, Inc., Sunnyvale, CA, 1990.

[16]Wertz, J. R., and Larson, W. J. (eds.), *Space Mission Analysis and Design*, Kluwer, Dordrecht, The Netherlands, 1991.

[17]Bryson, A. E., *Control of Spacecraft and Aircraft*, Princeton Univ. Press, Princeton, NJ, 1993.

[18]Griffin, M. D., and French, J. R., *Space Vehicle Design*, AIAA, Washington, D.C., 1991.

[19]Franklin, G. F., Powell, J. D., and Emami-Naeini, A., *Feedback Control of Dynamic Systems*, Addison–Wesley, Menlo Park, CA, 1987.